



Nanoscale

**Phase field approach for nanoscale interaction between
crack propagation and phase transformation**

Journal:	<i>Nanoscale</i>
Manuscript ID	NR-COM-07-2019-005960.R1
Article Type:	Communication
Date Submitted by the Author:	21-Oct-2019
Complete List of Authors:	Jafarzadeh, Hossein; Sharif University of Technology, Mechanical Engineering Levitas, Valery; Iowa State University , Department of Material Science and Engineering Farrahi, Gholam Hossein; Sharif University of Technology Javanbakht, Mahdi; Isfahan University of Technology,

SCHOLARONE™
Manuscripts

COMMUNICATION

Phase field approach for nanoscale interaction between crack propagation and phase transformation

Received 00th January 20xx,
Accepted 00th January 20xx

Hossein Jafarzadeh,^a Valery I. Levitas,^{*bc} Gholam Hossein Farrahi^{*a} and Mahdi Javanbakht^d

DOI: 10.1039/x0xx00000x

Phase field approach (PFA) to the interaction of fracture and martensitic phase transformation (PT) is developed, which includes change in surface energy during PT and the effect of unexplored scale parameter proportional to the ratio of the widths of the crack surface and the phase interface, both at nanometer scale. Variation of these two parameters causes unexpected qualitative and quantitative effects: shift of PT away from the crack tip, “wetting” of the crack surface by martensite, change in the structure and geometry of the transformed region, crack trajectory, and process of interfacial damage evolution, as well as transformation toughening. The results suggest additional parameters controlling coupled fracture and PTs.

Interaction between fracture and martensitic PTs is an extremely important problem in the physics and mechanics of strength, deformational, and transformational properties of materials. In particular, high stress concentration at the crack tip may cause PTs¹⁻⁵. PT absorbs energy and also produces transformation strain, which serves as a mechanism of plastic deformation and stress relaxation. Both increase resistance to the crack growth and ductility, which is called transformation toughening. Also, stresses generated during PTs may cause fracture. PFA has been widely used for modeling the complex microstructure evolution such as fracture⁶⁻¹⁰, PTs¹¹⁻¹⁵, and their interactions^{4, 16-20}. However, only few works¹⁸⁻²⁰ consider both fracture and PT with the PFA. In the current letter, we significantly advance the PFA to coupled fracture and PT by integrating it with PFA to surface-induced pre-transformations and transformations and including a new nanoscale effect (see ESI). PT¹³ and fracture⁸ are described with advanced models^{8,}

¹³, which in contrast to previous models^{18, 19}, satisfy some additional conditions to reproduce conceptually important features of stress-strain curves. Theory includes various coupling effects between fracture and PT. Thus, the suggested PFA is much more realistic than previous models^{18, 19}. The key point is that the theory possesses two characteristic nanoscale parameters: widths of the crack surface δ_c and the A-M interface width δ_p . We consider parameter $\bar{\delta}$ proportional to their ratio as the main dimensionless scale parameter in our formulation, and its effect is studied.

We found through the simulations that the reduction in the surface energy during PTs promotes nucleation of M at the crack tip, its stabilization as a nanolayer at the crack surface, or nucleation of the pre-martensite or M at the crack surfaces. Increase in surface energy during PT suppresses the PT near the crack tip and at the surfaces, and stress-induced PT occurs slightly away from the crack tip. In turn, change in surface energy of a solid during PT affects crack behavior in terms of change in cohesion and gradient energy, which changes crack nucleation location and trajectory. All these changes are essentially affected by the dimensionless width $\bar{\delta}$.

The subscripts 0, d, A, and M are for the undamaged solid, fully-damaged solid, austenite, and martensite, respectively. The PT and damage are described by the order parameters η and ϕ , respectively; both vary between zero and unity. The austenite (A) corresponds to $\eta=0$ and martensite (M) to $\eta=1$; the undamaged state is described by $\phi=0$ and fully damaged by $\phi=1$.

We consider PT between cubic austenite and tetragonal martensite in NiAl with transformation strain $\epsilon_t=(0.215, -0.078, -0.078)$ ¹⁴ and isotropic elasticity; other material parameters are given in the ESI. For these parameters, the width and energy of the phase interface are $\delta_p = 5.54 \sqrt{\beta_0/(2A_0(\theta^e - \theta^c))} = 1.5065 \text{ nm}$ and $E = \sqrt{\beta_0 A_0(\theta^e - \theta^c)}/18 = 0.2245 \text{ N/m}$ ²¹. Isotropic surface energies γ_A and γ_M vary in the range of 0.5-5 N/m and are presented below as $\bar{\gamma} = \gamma_M/\gamma_A$. Flow chart of the methodology is given in Figure S1 (see ESI).

^a Sharif University of Technology, School of Mechanical Engineering, Tehran 11365-11155, Iran.

^b Iowa State University, Departments of Aerospace Engineering and Mechanical Engineering, Ames, IA 50011, USA.

^c Ames Laboratory, Division of Materials Science and Engineering, Ames, IA, USA.

^d Isfahan University of Technology, Department of Mechanical Engineering, Isfahan 84156-83111, Iran

* Corresponding authors: (VIL) email: vlevitas@iastate.edu; (GHF) email: farrahi@sharif.edu.

Electronic Supplementary Information (ESI) available: [details of any supplementary information available should be included here]. See DOI: 10.1039/x0xx00000x

For the chosen cohesion energy ψ^c , the width of the crack surface $\delta_c = 1.14l^{\frac{2}{3}}$, where l is the initial distance between two planes forming crack surfaces. Thus, there are two characteristic widths, both at nanometer scale: width of the crack surface δ_c (or l) and the A-M interface width δ_p . We introduce $\bar{\delta} := 1.5(l/\delta_p)$ as the main dimensionless scale parameter in our theory. It was recently revealed that, for a free surface, such a ratio strongly affects the surface-induced martensitic PT²¹ and melting²² and is suggested as the new dimension in the phase diagram²². Generally, if any PFA includes two order parameters, their length scale ratio plays an essential role in the occurring different processes²³, e.g. for interaction between PT and dislocations¹⁵ and solid-solid PT via intermediate melt²². This parameter was never discussed for the fracture and, as is shown below, significantly affects PT and fracture processes. The plane stress problem is considered. Length, time, and stress dimensions were normalized by 1 nm, 1 ps, and 1 GPa, respectively.

Pseudoelastic behavior. Processes in a center cracked tension sample shown in Figure 1 are simulated at $\theta/\theta^e = 4.65$, i.e. deeply in the austenitic region in the *pseudoelastic regime*. An initial crack (bold line at the center) is introduced via an analytical solution⁸ for the damage parameter ϕ . An initial value of $\eta = 0.001$ is assumed everywhere. Homogeneous displacements u on the lateral edges are linearly increased to 1.125 nm in 0.075 ps and then remain constant. Due to the symmetry, only one-quarter of the sample is considered. Coupled PT and fracture are studied as function of $\bar{\gamma}$ keeping $\bar{\delta} = \text{const}$ and as a function of $\bar{\delta}$ keeping $\bar{\gamma} = \text{const}$.

Figure 2 shows the distribution of η ahead of the moving crack tip. Traditionally, PT starts around the crack tip, where stress concentration is the highest^{18, 19}. Here, the martensitic region is determined not only by the stress concentration but also by $\bar{\gamma}$ and $\bar{\delta}$. For $\bar{\gamma} \leq 1$ M exists at the crack tip. However, for $\bar{\gamma} = 10$ there is a residual A region around the crack tip with width $\approx \delta_c$, because of its much lower surface energy. This is a new regime for the coupled crack and transforming zone propagation. Larger $\bar{\delta} = 10$ increases the width of the A layer and suppresses martensitic PT, making M incomplete (premartensite) in the entire transforming zone, which is smaller than for $\bar{\delta} = 1$.

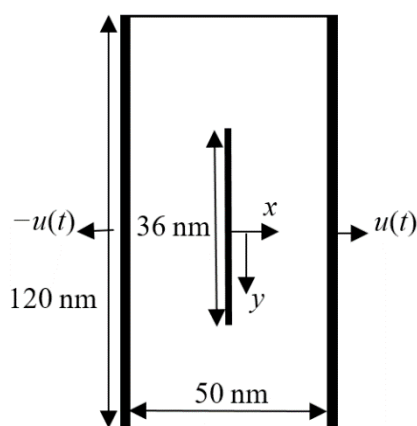


Figure 1. Schematics of the center cracked tension sample with the boundary conditions.

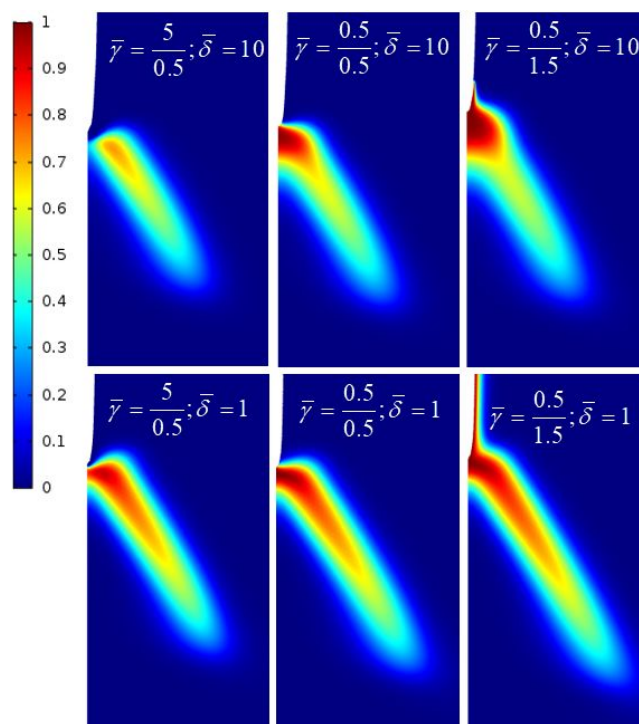


Figure 2. PT region described by the distribution of the order parameter η ahead of the moving crack tip at time $t=2$, shown in the region $[x,y]=[(0, 10), (25, 45)]$ for different $\bar{\gamma}$ and $\bar{\delta}$ (shown in figures) for the pseudoelastic regime. The region with $\phi \geq 0.99$ is eliminated from the figures and is shown as the crack.

For $\bar{\gamma} = 1$, the martensitic region is larger and transformation is more complete than for $\bar{\gamma} = 10$. For both cases, the martensitic structure moves together with the crack tip, and the material undergoes direct and reverse PTs due to pseudoelastic behavior. Such a behavior is typically observed in an experiment for a pseudoelastic material which has a crack⁵. For $\bar{\gamma} = 1/3$, the martensitic region grows further and resides at the crack surface, promoted by reduction of the surface energy during PT. For the thicker crack surface, M cannot propagate far away from the stress concentrator, but for the thinner crack surface, M propagates along the entire crack surface, i.e. “wets” it. This thin M layer is induced and stabilized by the surface after unloading deep in the region of stability of A. Such a residual M at crack and notch surfaces were observed experimentally for NiTi single crystal². Thus, the traditionally-neglected scale parameter $\bar{\delta}$ essentially affects martensitic PT at the crack tip and crack propagation.

Pseudoplastic behavior. Similar problems are solved to study *pseudoplastic* behavior at $\theta = \theta^e$ for which residual M exists after local unloading. We changed the barrier parameter A_0 to keep the same barrier height \bar{A} and, consequently, the magnitude of the stress for the direct PT (see ESI for definitions of the material parameters).

In Figure 3 for $\bar{\gamma} = 1$, when the surface energy does not have any contribution to the driving force for PT, the PT starts at the crack tip and the transformed region grows with the crack propagation, i.e. reverse PT does not occur behind the crack tip. This corresponds to known experiments¹. For $\bar{\gamma} = 10$, smaller surface energy of A drives the reverse PT near the crack tip. This is a new effect for stress-induced PT during crack

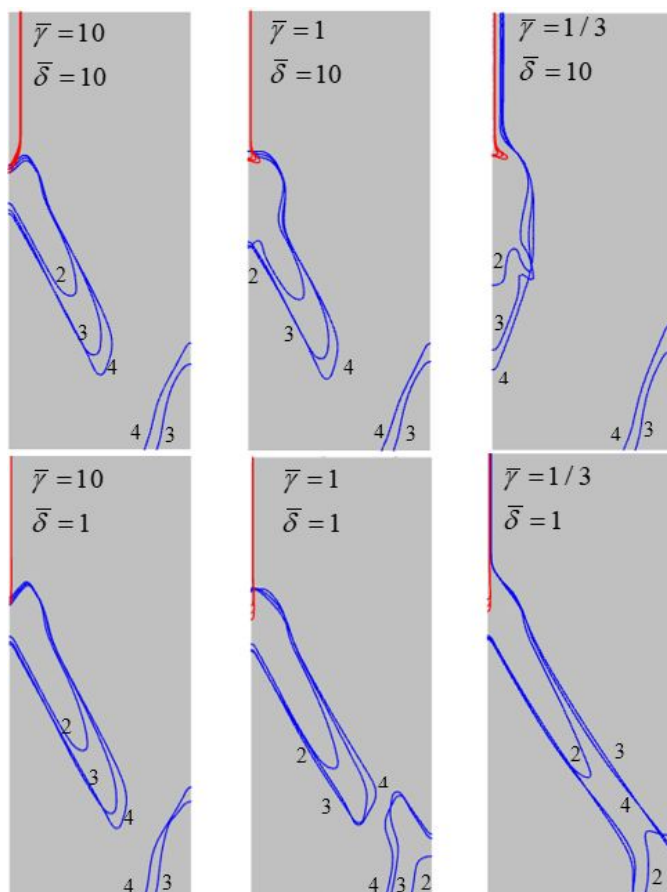


Figure 3. PT region (distribution of η) ahead of the moving crack tip for different $\bar{\gamma}$ and $\bar{\delta}$ for the pseudoplastic regime. Red and blue lines show contour lines $\phi=0.5$ and $\eta=0.5$, respectively, for $t=2, 3$, and 4 (shown near curves).

growth for the pseudoplastic regime. For $\bar{\gamma} \leq 1$, the reverse PT does not occur; in addition, reduction of the surface energy leads to a surface-induced martensitic PT along the entire crack surface. Our results also show significant effects of the scale parameter $\bar{\delta}$. For $\bar{\gamma} = 10$, there is a residual austenite region around the crack tip, and smaller $\bar{\delta}$ results in the larger transformed region. However, in contrast to the pseudoelastic regime, martensitic PT is completed in the entire transformed region. For $\bar{\gamma} \leq 1$, the morphology of the transformed regions is entirely different for different $\bar{\delta}$. For larger $\bar{\delta}$, there is more M near the crack tip and along the crack surface and less in the growing-in-bulk-M plate. Promotion of the M by thicker crack surface relaxes stresses, suppressing martensite growth in the plate. Also, *crack branching* is observed for larger $\bar{\delta}$.

Interfacial fracture. Here we solve the problem for the same geometry and boundary conditions, shown in Figure 4, but the right side of the sample is initially martensite, i.e. *interfacial crack* is considered at $\theta = \theta^e$. The M was introduced by means of the analytical solution for the equilibrium interface¹⁴. A tensile misfit strain of 0.215 in M produces significant vertical compressive stress in M and tensile stress in A. To avoid the $A \leftrightarrow M$ PT and focus on the interfacial crack propagation, we used $L_\eta \ll L_\phi$, where L_ϕ and L_η are the kinetic coefficients for damage and PT, respectively. Results will be also interpreted in terms of Griffith theory for crack propagation,

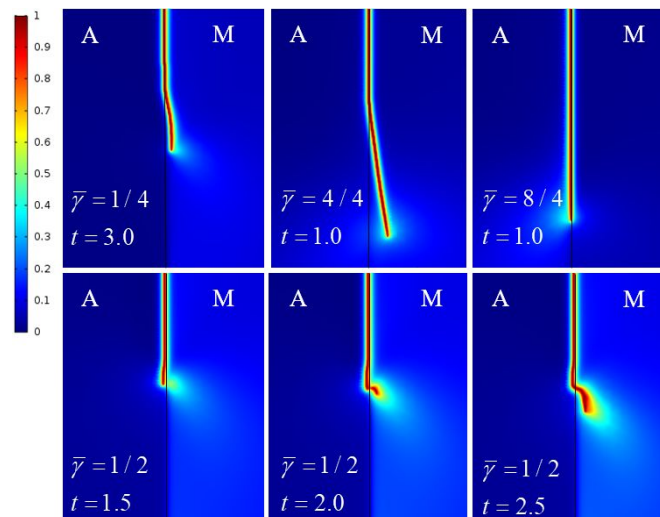


Figure 4. Damage distribution ϕ within and outside the phase interface shown in the region $[x,y]=[-10 10],[25 50]$ for $\bar{\delta}=1$ and different conditions shown in figures.

$$J > \Delta\gamma \text{ with } \Delta\gamma = 2\gamma_M \text{ or } 2\gamma_A \text{ or } \Delta\gamma = \gamma_M + \gamma_A - E, \quad (1)$$

where J is elastic energy release, and three options for the change in surface energy of a crack $\Delta\gamma$ are for crack propagating through M, A, or A-M interface, respectively.

Despite the symmetry in the loading and geometry, the crack path is not straight. For $\bar{\gamma} = 1/4$, the crack deviates to the martensitic region due to much smaller $\Delta\gamma$. For $\bar{\gamma} = 1/2$, the crack is initially directed to the A driven by tensile stresses due to misfit strain, i.e. by larger J despite the larger $\Delta\gamma$. Relaxation of internal stresses due to misfit and generation of tensile stresses near the crack tip leads to significant damage in the weaker M. Next, crack turns and propagates in the M, governed by smaller $\Delta\gamma$. For $\bar{\gamma} = 4/4$, when $\gamma_M = \gamma_A \gg E$, termination of the lattice misfit at the crack surfaces produces a stress field and J , which lead to a deviation of the crack into M. For $\bar{\gamma} = 8/4$, larger γ_M suppresses this deviation, leading to the interfacial crack propagation. Thus, interplay between initial stresses due to a lattice misfit at the A-M interface and different surface energies of A and M result in different crack propagation scenarios.

Crack nucleation. To study crack nucleation in Figure 5, the finite-width A-M interface was introduced using the analytical solution, but transformation strain was neglected. An initial value of $\phi=0.01$ is applied. The upper edge of a sample and the notch surface are stress-free; the right side is moved with $u(\text{nm})=2t(\text{ps})$, the left side is fixed in the horizontal direction, and the lower left corner point is fixed. Vertical displacement at the lower horizontal plane is zero ($v=0$). Eq. (1) will be utilized for the interpretation of the results.

For cases (a) and (b), the lowest $\Delta\gamma$ in equation $J > \Delta\gamma$ leads to barrierless crack nucleation and propagation in A and along the interface, respectively. For case (a), the lower surface energy of A leads to crack nucleation and propagation in A, even though disappearance of interface energy increases the driving force for crack growth within the interface. For cases (b)-(d), energies of A and M are equal. For case (b), the stress concentrator due to notch and the disappearance of the interface energy both lead to crack nucleation along the interface. In case (c), the effect of interface

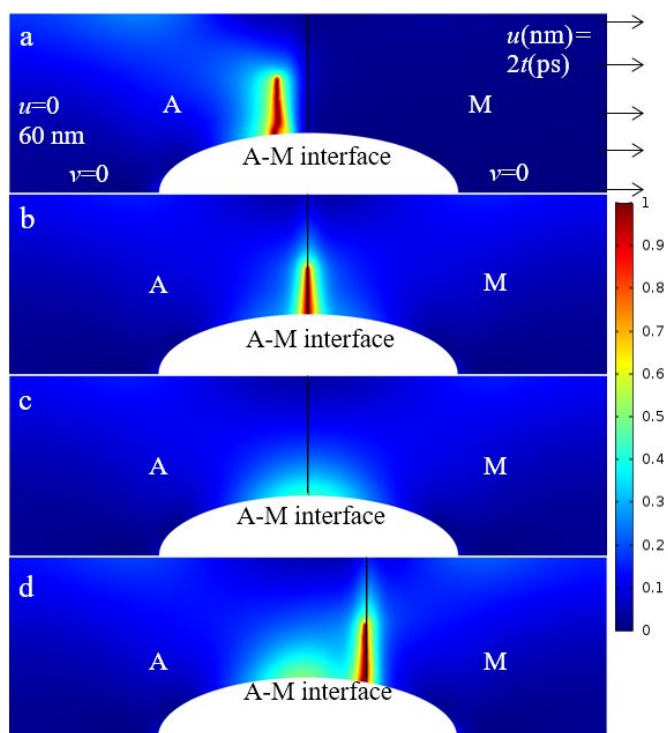


Figure 5. Damage distribution ϕ within/near the phase interface for: a) $\bar{\gamma} = 5/0.5$, $t=2.8$; b) $\bar{\gamma} = 0.5/0.5$, $t=2.5$; c) $\bar{\gamma} = 0.5/0.5$, $t=2.5$, without interface energy ($A_0 = \beta_0 = 0$ in Eq. (12) in ESI), and d) $\bar{\gamma} = 0.5/0.5$, $t=2.8$. The interface ($\eta=0.5$) is shown by a solid black line in each figure.

energy on the crack driving force is neglected, leading to larger $\Delta\gamma$; thus, for the same loading as in case (b), the crack does not nucleate. For case (d), while the stress concentration due to notch and J are larger in the middle of the sample than at the interface, the disappearance of interface energy is dominant, and the crack propagates through the interface due to smaller $\Delta\gamma$. Again, interplay between stress concentration, different surface energies of A and M, and disappearance of the energy of the pre-existing A-M interface produce variety of crack nucleation and evolution developments.

Transformation toughening. The easiest way to evaluate the transformation toughening is by comparing crack tip velocity for the cases without PT and different PT scenarios. This is collected in Table 1 for simulations in Figure 2 in pseudoelastic regime.

Due to the complex and nonlinear interplay of all parameters involved in the Ginzburg-Landau equations, there is no straightforward relationship between the extension of PT in Figure 2 and the results in Table 1. For all cases, PT significantly reduces crack speed. The largest transformation toughening is for $\bar{\gamma} = 10$, when A is located at the crack tip and surfaces; the second largest crack velocity reduction is for $\bar{\gamma} = 1/3$, when M “wets” part of the entire crack surface; and the smallest influence of PT is for $\bar{\gamma} = 1$. The largest effect of the parameter $\bar{\delta}$ is within 9% for $\bar{\gamma} = 10$; this effect is nonmonotonous.

	$\bar{\gamma} = \frac{5}{0.5}$	$\bar{\gamma} = \frac{0.5}{0.5}$	$\bar{\gamma} = \frac{0.5}{1.5}$	no PT, $\gamma_A=0.5$ N/m
$\bar{\delta} = 10$	1.13	1.33	1.19	1.82
$\bar{\delta} = 5$	1.03	1.26	1.20	1.82
$\bar{\delta} = 1$	1.05	1.29	1.22	1.82

Table 1. Crack tip velocity for different cases (nm/ps)

Conclusions

An advanced PFA to the interaction between fracture and martensitic PT is developed with nontrivial couplings, explicitly incorporating surface-induced PT and pretransformation as well as the scale effect related to the ratio of the width of the crack surface to the width of the phase interface. It was demonstrated that the effect of these parameters on the PT and fracture is quite strong and multifaceted. In particular, lower surface energy of M than of A can cause surface-induced PT and pretransformation at the crack surface (“wetting” by martensite) even in the pseudoelastic regime, when unloading near the crack surface should cause the reverse PT. In contrast, lower surface energy of A than of M suppresses the PT at the crack tip and shifts M away from the region of the highest stress concentration in the pseudoelastic regime, and causes reverse PT to A at the crack tip in the pseudoplastic regime. The geometry and internal structure of the transformed region strongly depend on the parameter $\bar{\delta}$ in both regimes. Parameters $\bar{\gamma}$ and $\bar{\delta}$ essentially affect crack trajectory (branching) and the process of interfacial damage evolution, as well as transformation toughening, i.e. these are new parameters controlling coupled fracture and PTs, and probably twinning^{24, 25}.

Two different interpretations of the widths of interfaces and surfaces are used in the phase-field approach. In one of them, they are just regularization parameters without physical meaning. Our results show that the regularization lengths cannot be chosen arbitrarily because their ratio significantly affects the results of simulations. Alternatively^{14, 21-23, 26, 27}, these are actual nanometer-size widths of interfaces, surfaces, intermediate phases within interfaces, dislocation bands, and pretransformed layers, which are determined using atomistic simulations and experiments. For example, for surface melting of Al nanoparticles, $\bar{\delta}$ was determined by fitting phase-field approach results to the size-dependent melting temperature²². Widths of surface disordered/molten layer and of intermediate phases are determined as well^{26, 28, 29}. For this case, the obtained results represent real physical effects. For surface-induced martensitic transformations, widths of surface layer and surface energies of A and M are unknown⁴. These parameters, as well as width and energy of A-M interface, depend on composition, point defect segregation, dislocation structure at external surfaces and interfaces, and can be partly controlled.

Note that phase interface width in Si can be changed from a nanometer to infinity (i.e., leading to a homogeneous interface-free transformation) by applying special triaxial stresses⁵. We hope

that our theoretical predictions will attract experimental efforts to determine material parameters and study predicted phenomena. Review article²³ is devoted solely to the effect of δ in various material processes. Note that the results of phase-field approach to surface-induced martensitic phase transformations²¹ and obtained surface structures may be observed at the crack surfaces as well.

Conflicts of interest

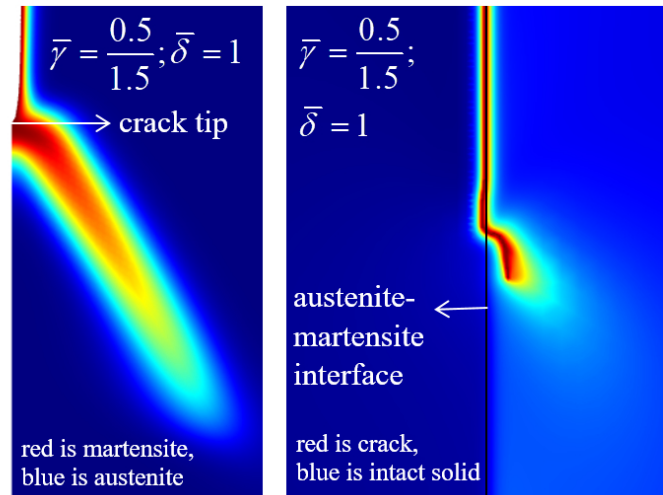
The authors declare no competing financial interest.

Acknowledgements

HJ acknowledges the support of Sharif University of Technology, Nano Foundation and Ministry of Science, Research and Technology of Iran. VIL acknowledges the support of the ONR (N00014-19-1-2082), NSF (DMR-1904830), ARO (W911NF-17-1-0225), and ISU (Vance Coffman Faculty Chair Professorship).

References

- U. D. Hangen and G. Sauthoff, *Intermetallics*, 1999, **7**, 501-510.
- A. Kreuziger, L. J. Bartol, K. Gall and W. C. Crone, *Journal of the Mechanics and Physics of Solids*, 2008, **56**, 2896-2905.
- S. Gollerthan, M. L. Young, K. Neuking, U. Ramamurty and G. Eggeler, *Acta Materialia*, 2009, **57**, 5892-5897.
- M. Mamivand, M. Asle Zaeem and H. El Kadiri, *Acta Materialia*, 2014, **64**, 208-219.
- G. M. Vasko, Ph.D. Thesis, University of Minnesota, Minnesota, 2001.
- A. Karma, D. A. Kessler and H. Levine, *Physical Review Letters*, 2001, **87**, 045501.
- H. Henry and H. Levine, *Physical Review Letters*, 2004, **93**, 105504.
- V. I. Levitas, H. Jafarzadeh, G. H. Farrahi and M. Javanbakht, *International Journal of Plasticity*, 2018, **111**, 1-35.
- G. H. Farrahi, M. Javanbakht and H. Jafarzadeh, *Continuum Mechanics and Thermodynamics*, 2018, DOI: 10.1007/s00161-018-0685-z.
- H. Jafarzadeh, G. H. Farrahi and M. Javanbakht, *Continuum Mechanics and Thermodynamics*, 2019, DOI: 10.1007/s00161-019-00775-1, 1-13.
- Y. M. Jin, A. Artemev and A. G. Khachaturyan, *Acta Materialia*, 2001, **49**, 2309-2320.
- T. Lookman, A. Saxena and R. C. Albers, *Physical Review Letters*, 2008, **100**, 145504.
- V. I. Levitas and D. L. Preston, *Physical Review B*, 2002, **66**, 134206.
- V. I. Levitas, D. L. Preston and D.-W. Lee, *Physical Review B*, 2003, **68**, 134201.
- V. I. Levitas and M. Javanbakht, *Nanoscale*, 2014, **6**, 162-166.
- A. Boulbitch and A. L. Korzhenevskii, *The European Physical Journal B*, 2016, **89**, 261.
- A. Boulbitch, Y. M. Gufan and A. L. Korzhenevskii, *Physical Review E*, 2017, **96**, 013005.
- R. Schmitt, C. Kuhn, R. Skorupski, M. Smaga, D. Eifler and R. Müller, *Archive of Applied Mechanics*, 2015, **85**, 1459-1468.
- T. Zhao, J. Zhu and J. Luo, *Engineering Fracture Mechanics*, 2016, **159**, 155-173.
- J. Clayton and J. Knap, *Continuum Mechanics and Thermodynamics*, 2018, **30**, 421-455.
- V. I. Levitas and M. Javanbakht, *Physical Review Letters*, 2011, **107**, 175701.
- V. I. Levitas and K. Samani, *Physical Review B*, 2014, **89**, 075427.
- V. I. Levitas, *Scripta Materialia*, 2018, **149**, 155-162.
- J. D. Clayton and J. Knap, *Acta Materialia*, 2013, **61**, 5341-5353.
- J. D. Clayton and J. Knap, *Computer Methods in Applied Mechanics and Engineering*, 2016, **312**, 447-467.
- B. Pluis, D. Frenkel and J. F. van der Veen, *Surface Science*, 1990, **239**, 282-300.
- V. I. Levitas and M. Javanbakht, *Physical Review Letters*, 2010, **105**, 165701.
- J. Luo, *Critical reviews in solid state and materials sciences*, 2007, **32**, 67-109.
- B. Pluis, A. D. Van der Gon, J. Frenken, van der Veen and JF, *Physical Review Letters*, 1987, **59**, 2678.
- V. I. Levitas, H. Chen and L. Xiong, *Physical Review Letters*, 2017, **118**, 025701.



Phase field approach to interaction of fracture and phase transformation is developed including scale effects and change in surface energy.